Surface & Coatings Technology 355 (2018) 169–173

Contents lists available at ScienceDirect

Surface & Coatings Technology

journal homepage: www.elsevier.com/locate/surfcoat

Very high fluence nitrogen implantations in metals studied by Rutherford Backscattering Spectrometry

J. Cruz[a,*], H. Silva[a], J. Lopes[b], J. Rocha[c], A.P. Jesus[a]

[a] Laboratório de Instrumentação, Engenharia Biomédica e Física da Radiação (LIBPhys-UNL), Departamento de Física, Faculdade de Ciências e Tecnologia da Universidade Nova de Lisboa, Monte da Caparica, 2892-516 Caparica, Portugal
[b] Instituto Superior de Engenharia de Lisboa, GIAAPP/ISEL, Lisboa, Portugal
[c] Laboratório de Aceleradores e Tecnologias de Radiação, IST, Universidade de Lisboa, Portugal

ARTICLE INFO

Keywords:
Nitrogen implantation
RBS
Deficiency method
Stopping power

ABSTRACT

This paper reports a study of $^{14}N^{+}$ implanted Ti and Zr films analysed by Rutherford Backscattering Spectrometry (RBS). The fluences ranged from 4.0–10.0 × 10^{17} atoms·cm^{-2} and energies of 15–20 keV. Here, the nitrogen depth distributions were obtained simultaneously and independently for each RBS spectrum from the direct nitrogen signal and from the reduction of the backscattered yield from Ti and Zr (deficiency method). Fits to the RBS spectra show that the deficiency method clearly underestimates the ^{14}N yield by 32% for Ti (and 45% for Zr) when compared to the direct nitrogen signal. This discrepancy reduces to 23% for Ti (and 43% for Zr) when the presence of nitrogen bubbles are simulated in the fits.

1. Introduction

Very high fluence ion implantation is a well-known and effective solution for enhancing the lifetime and improving the performance of metallic tools [1]. N^{+} is the most common ion used in the metallurgical industry since it promotes the fixing of micro cracks, the filling of lattice spaces in the metallic structure and the formation of nitride compounds [1]. This results in new surface lattice properties that improve mechanical (wear, friction, hardness, adhesion, fatigue) and chemical (corrosion, oxidation, electrochemistry, catalysis) behaviours [2–4]. The degree of surface modification by nitrogen ion implantation depends on the ion energy, current density, irradiation time and the substrate temperature. Ion energies are typically set to around 20–30 keV, meaning a range of hundreds of angstroms in metals as given by the SRIM code [5].

For these ranges, Rutherford Backscattering Spectrometry (RBS) can effectively quantify non-destructively the material in the implanted volume, with a depth resolution of a few tens of nanometre and with an uncertainty that can be as good as ~5%. The higher source of uncertainty in RBS calculations results from the fact that backscattered yields from implanted nitrogen ions can hardly be observed because they are hidden by the yields of metals with a heavy mass (RBS sensitivity is proportional to the square of the atomic number). For example, on the assumption N/Zr = 1, the backscattered yield of nitrogen atoms increases by ~2% the yield of Zr atoms in the backscattering energy region of nitrogen. Therefore, it is difficult to use the nitrogen yields for the calculation of atomic yields. In these cases, the deficiency method can be applied, i.e., the nitrogen depth profile can be extracted from the reduction of the backscattered yields from host metal atoms induced by the change in stopping cross section owing to the nitrogen atoms [6]. RBS has been used consistently in the past decades by different authors for the determination of the N^{+} retained fluence and depth distribution in the metallic substrate [7–9]. However, some works [7,8] have shown that RBS results are not always in agreement with other quantification techniques like Auger Electron Spectroscopy [7] or X-ray Diffraction (XRD) [8].

In order to try to understand the reason for these differences and also to verify the sensitivity of the deficiency method, thin Ti and Zr films deposited on Be foils were implanted with ^{14}N ions. This allowed avoiding the superposition of the ^{14}N and the metal backscattered yields, and therefore the ^{14}N implanted can be characterised simultaneously and independently in the same RBS spectrum from the direct nitrogen signal and from the deficiency method. The thick Be backing was chosen because being lighter than nitrogen, its backscattered yield does not interfere with the nitrogen yield.

2. Material and methods

The Zr and the Ti samples were deposited by reactive rf magnetron sputtering from a high purity Zr and Ti targets, respectively, onto

* Corresponding author.
E-mail address: jdc@fct.unl.pt (J. Cruz).

https://doi.org/10.1016/j.surfcoat.2018.01.042
Received 31 October 2017; Received in revised form 10 January 2018; Accepted 13 January 2018
Available online 03 February 2018

Beryllium foils with a purity of 99.0% from Goodfellow [10] with dimensions: 12.5 × 12.5 × 0.5 mm^3. Be substrates were ultrasonically cleaned and sputter etched for 15 min in a 0.4 Pa Ar atmosphere (200 W rf power). Depositions were carried out under an Ar atmosphere in an Alcatel SCM650 apparatus located at the Research Centre on Interfaces and Surface Performance (Guimarães, Portugal). The base pressure in the deposition chamber was about 10^{-6} mbar and rose to values around 4×10^{-3} mbar during depositions. ZrN and TiN samples were also deposited on Be foils, under the same experimental conditions. These samples were used as control samples.

The Ti and Zr samples were implanted with ^{14}N ions at the DANPHYSIK ion Implanter at CTN/IST (Lisbon, Portugal) [11]. The ion beam was scanned over the samples to achieve a uniform implantation. For the Ti-Be sample, two implantations were performed: Implantation 1: Energy = 20 keV, nominal fluence = 2.0×10^{17} atoms·cm^{-2}, current density = 12.5 μA·cm^{-2} (colour of the Ti surface after implantation: bulk Ti); Implantation 2: Energy = 15 keV, nominal fluence = 2.0×10^{17} atoms·cm^{-2}, current density = 16.7 μA·cm^{-2} (colour of the Ti surface after implantation: light gold – almost TiN bulk colour). For the Zr-Be sample, one implantation was performed: Energy = 20 keV, nominal fluence = 1.0×10^{18} atoms·cm^{-2}, current density = 16.0 μA·cm^{-2} (colour of the Zr surface after implantation: light gold – almost ZrN bulk colour).

RBS spectra were obtained under vacuum conditions (P ≈ 5×10^{-6} mbar) at the nuclear reactions beam line of the 2.5 MV Van de Graaff Accelerator of the CTN/IST using a 2.0 MeV $^4He^+$ beam at normal incidence angle. The RBS spectra were collected by a 50 mm^2 PIPS detector with a 20 keV resolution in Cornell geometry placed at 162° to the beam direction. The RBS spectra measured before and after $^{14}N^+$ implantations were fitted by means of the DataFurnace code [12], including the beam straggling calculated by the Chu correction with the Tschälar effect, the double scattering contribution and the pulse pile-up effect (considering the Molodtsov and Gurbich algorithm [13]). Prior to doing the fits, each RBS spectrum was manipulated in order to remove the background signal below the nitrogen peak. Fig. 1 shows an example of this manipulation for the Ti-Be sample after the $^{14}N^+$ implantations. The red line in Fig. 1a) represents the background line and results from a succession of fits with exponential functions. The oxygen peak (also in red) was fitted with a Gaussian with a Lorentzian tail. Fig. 1b) highlights the RBS spectrum region where the background subtraction was implemented (region where the carbon, nitrogen and oxygen signals are present).

The nitrogen signal quantification has a statistical uncertainty associated to the number of counts, N_C, observed in the ^{14}N region, and a systematic uncertainty resulting from the estimation of the number of background counts, N_B. The statistical uncertainty is just the square root of the number of counts. The systematic uncertainty is estimated from comparing the background yield obtained with this multi-fit approach (Fig. 1) and a straight-line subtraction under the nitrogen peak. Table 1 shows the uncertainty values obtained for the Ti-Be and the Zr-Be samples. The relative uncertainties presented in this table will be used to compute the quoted uncertainties in the next section, using the direct method.

In turn, the uncertainty associated to the nitrogen quantification using the deficiency method has also a statistical component, given by the square root of the number of Ti or Zr counts in the spectrum region altered by the presence of nitrogen, and a systematic component determined from the visual inspection to the Ti or Zr simulated yields: small changes in these elements concentrations are simulated and a visual comparison is done between the experimental yield and the simulated curve. In this case, the uncertainty is set at the limit where the agreement between experimental points and simulated curve is clearly broken. Table 2 gives the uncertainty values obtained for the Ti-Be and the Zr-Be samples. The relative uncertainties presented in this table will be used to compute the quoted uncertainties in the next section, using the deficiency method.

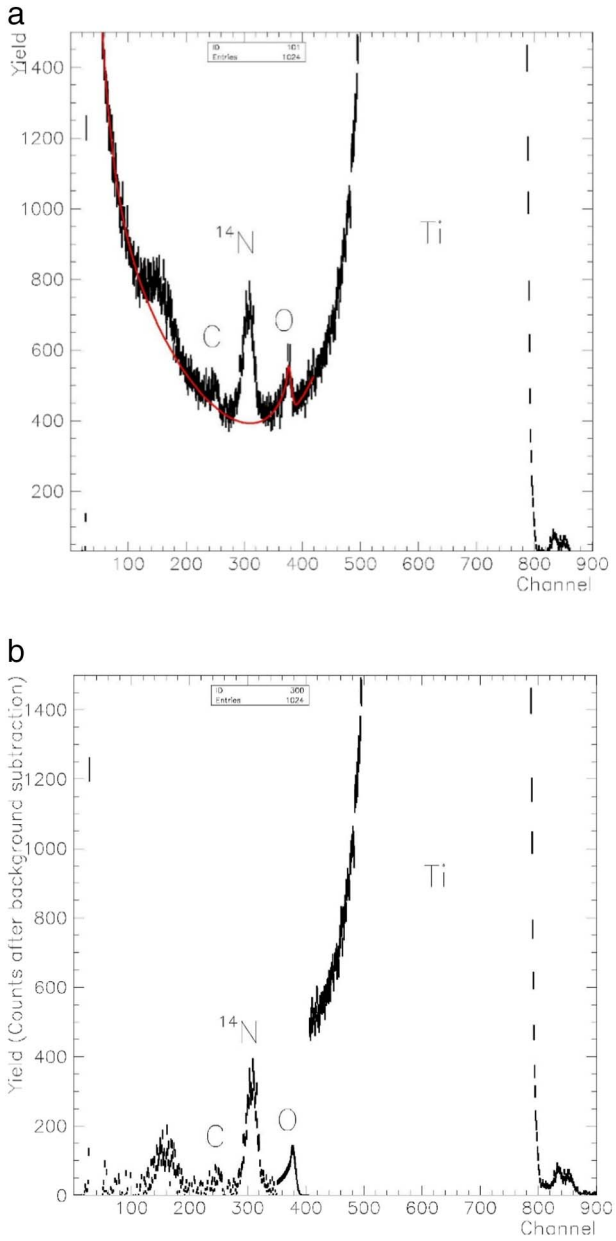

Fig. 1. a) – RBS spectrum (partial) for the Ti-Be sample after the ^{14}N implantations. The red line in represents the background line and results from a succession of fits with exponential functions. The oxygen peak (also in red) was fitted with a Gaussian with a Lorentzian tail.
b) – RBS spectrum (partial) after the background subtraction in the C, ^{14}N and O signals region. (For interpretation of the references to colour in this figure legend, the reader is referred to the web version of this article.)

Table 1
Direct method - statistical and systematic uncertainties for the Ti-Be and Zr-Be samples.

Sample	Statistical uncertainty			Systematic uncertainty		
	N_C	$\sqrt{N_C}$	$\sqrt{N_C}/N_C$	N_B (multi-fit)	N_B (straight line fit)	Ratio of N_B
Ti-Be	28,328	168.3	0.6%	20,442	21,383	4.6%
Zr-Be	9086	95.3	1.0%	4242	4391	3.5%

Table 2
Deficiency method - statistical and systematic uncertainties for the Ti-Be and Zr-Be samples.

Sample	Statistical uncertainty			Systematic uncertainty
	N_C	$\sqrt{N_C}$	$\sqrt{N_C}/N_C$	
Ti-Be	212,851	461	0.2%	2.3% in Ti ⇒ 4.5% for ^{14}N
Zr-Be	269,264	519	0.2%	2.8% in Zr ⇒ 3.9% for ^{14}N

3. Results and discussion

3.1. Before implantations

Before implantation the Ti-Be and Zr-Be samples were analysed by RBS. The analysis of the two RBS spectra gave for the deposited Ti film a thickness of 2.90×10^{18} atoms·cm^{-2} (=510 nm, assuming the bulk Ti density which is 5.681×10^{22} atoms·cm^{-3}), and for the deposited Zr film a thickness of 1.55×10^{18} atoms·cm^{-2} (=362 nm, assuming the bulk Zr density which is 4.285×10^{22} atoms·cm^{-3}). In both spectra, it was also detected small amounts of carbon and oxygen. No signal of nitrogen was detected.

The RBS spectra obtained for the TiN-Be and ZrN-Be samples are consistent with a 1:1 stoichiometry for the nitrides with thicknesses around 40 nm (assuming the bulk densities).

Fig. 2a) shows the RBS spectrum measured for the TiN-Be sample (open squares). In the fit to this spectrum, performed with DataFurnace (red line), a fixed $Ti_{0.49}N_{0.51}$ stoichiometry was obtained. C, O and Ar, whose signals are clearly visible, as well, were also considered in the fit. The nitrogen signal yields a thickness of $N_N = 2.1 \times 10^{17}$ atoms·cm^{-2}. A direct calculation using the nitrogen and the titanium peak areas ($Y_N/Y_{Ti} = N_N/N_{Ti} \times \sigma_N^{Ruth}/\sigma_{Ti}^{Ruth}$) also gives $Ti_{0.49}N_{0.51}$. Fig. 2b) and a) zoom in Fig. 2a) in the nitrogen and in the titanium signal regions, respectively. Fig. 2d) gives the depth profiles for $Ti_{0.49}N_{0.51}$, C, O, Ar and Be obtained from the fit of Fig. 2a). It was used seven layers to do the fit, and for each layer, the concentrations are fixed as depicted in Fig. 2d).

3.2. After implantations

3.2.1. Ti-Be sample

Fig. 3 shows the results from the fit to the RBS spectrum measured for the Ti-Be sample after the second implantation. The elements considered in this fit are Ti, ^{14}N, C, O and Be comprised in 19 layers – Fig. 3c). In opposition to what was obtained for the TiN fit of Fig. 2, Fig. 3a) and b) show that a simultaneous fit to the ^{14}N and the Ti signals is not possible, meaning that there is no agreement between the direct method and the deficiency method to obtain the retained fluence and the depth distribution for nitrogen. The direct fit to the ^{14}N signal [green line in Fig. 3a) and b)] gives a retained fluence of [2.80 ± 0.02 (stat) ± 0.13 (syst)] × 10^{17} atoms·cm^{-2} (=70% of the nominal fluence) while the fit to the Ti signal [red line in Fig. 3a) and b)] gives a ^{14}N retained fluence of [1.89 ± 0.00 (stat) ± 0.09 (syst)] × 10^{17} atoms·cm^{-2} (=47% of the nominal fluence). This means that the deficiency method gives a ^{14}N yield that is 32% lower when compared with the direct quantification of the ^{14}N signal. These fits were performed considering a homogeneous nitrogen distribution. However, it is known that for very high fluence nitrogen implantations, bubbles of this gas are formed inside the metallic volume. So, in order to quantify how nitrogen bubbles might affect the shape of the RBS spectrum, it was added to the DataFurnace input parameters, instructions to simulate bubbles (spheres) of ^{14}N with 10 nm radius, randomly distributed occupying a volume fraction that ranged from 0% to 60% depending on the nitrogen concentration calculated for each of the 19 layers (other bubble radius and volume fractions were simulated with DataFurnace, but the agreement with experimental data got worse). In Fig. 3, it is also shown the results from the simulation considering the nitrogen bubbles [blue line in Fig. 3a) and b)]. Here, the fit to the Ti signal gives a ^{14}N retained fluence of [2.15 ± 0.00 (stat) ± 0.10 (syst)] × 10^{17} atoms·cm^{-2} (=54% of the nominal fluence). With this recalculated ^{14}N yield, we have that the deficiency method gives a ^{14}N yield which is now 23% lower when compared from the direct quantification of the ^{14}N signal. So, the simulation of nitrogen bubbles inside the Ti film reduces the discrepancy between the direct and the deficiency method ^{14}N quantifications, validating their presence. Fig. 3c) gives the depth profiles for Ti, ^{14}N, C and O obtained from the fit to the

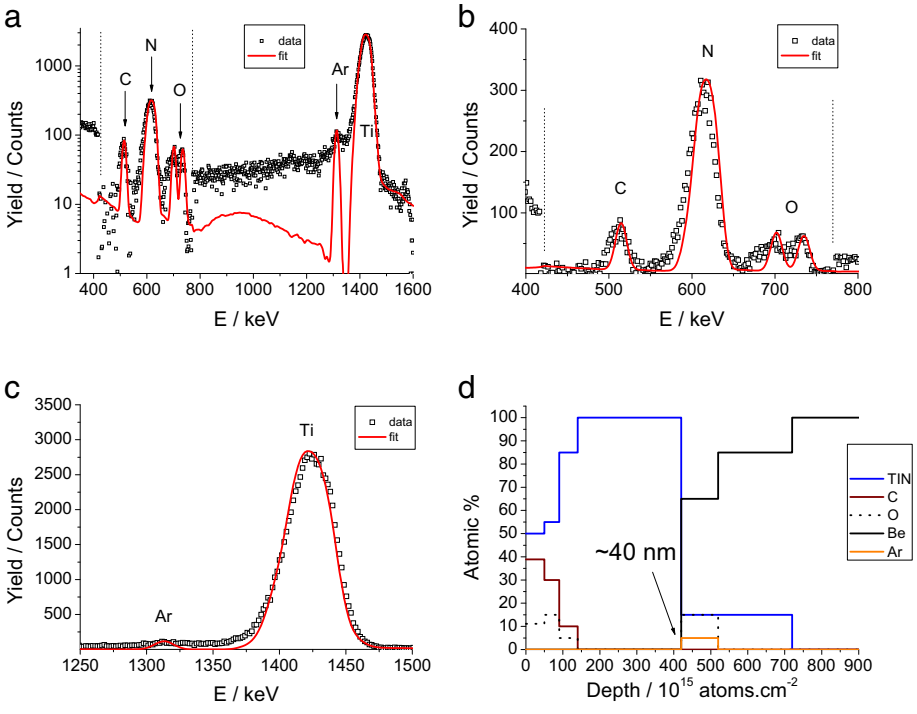

Fig. 2. a) – RBS spectrum taken for the TiN-Be sample. Spectrum fitted with DataFurnace code.
b) – Fig. 2a zoom in: C, N, O region.
c) – Fig. 2a zoom in: Ti region.
d) – Elemental depth profiles for TiN, C, O, Be and Ar obtained from the RBS spectrum fit of Fig. 2a.

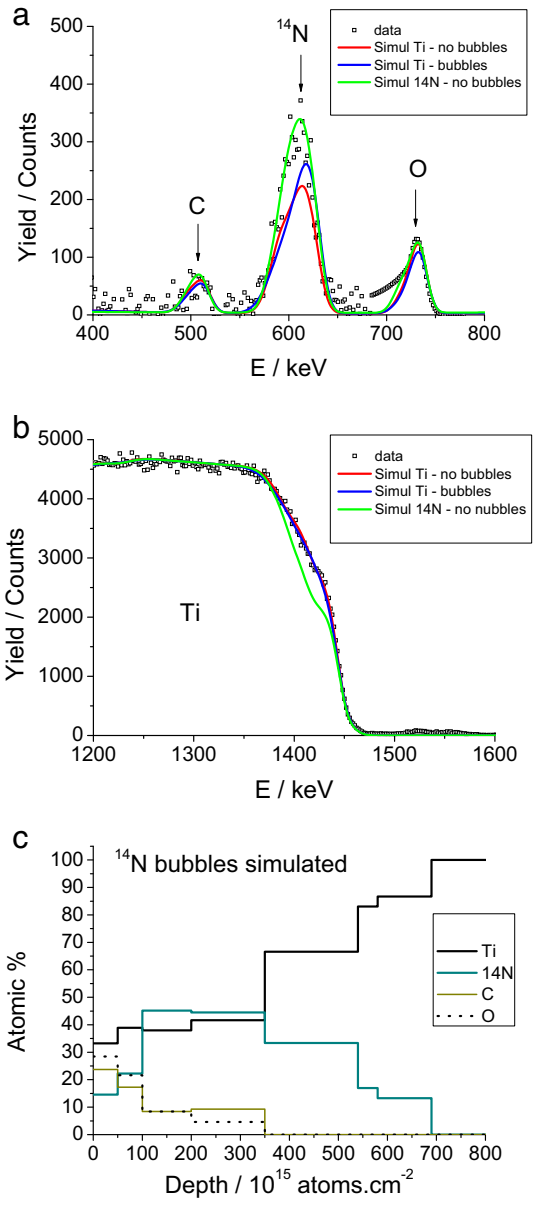

Fig. 3. a) – Partial RBS spectrum (C, ^{14}N, O region) taken for the Ti-Be sample after the ^{14}N implantations. The spectrum was fitted with DataFurnace code considering three situations. i) Green line (direct method): a good fit to the ^{14}N signal is obtained with a significant Ti yield reduction not described by experimental data, as shown in Fig. 3b. ii) Red line: deficiency method fit without considering the formation of nitrogen bubbles. The Ti signal is well-simulated (Fig. 3b), but the ^{14}N expected yield dropped by 32% as compared with the direct method fit (green line). iii) Blue line: deficiency method fit simulated with nitrogen bubbles. The Ti signal is well-simulated (Fig. 3b), but the ^{14}N expected yield dropped by 23% as compared with the direct method fit (green line).
b) – Partial RBS spectrum (Ti region) taken for the Ti-Be sample after the ^{14}N implantations. The spectrum was fitted with DataFurnace code considering three situations. i) Green line: direct method ^{14}N fit. ii) Red line: deficiency method fit without considering the formation of nitrogen bubbles. iii) Blue line: deficiency method fit simulated with nitrogen bubbles.
c) – Elemental depth profiles for Ti, ^{14}N, C and O obtained from the RBS spectrum fit of Fig. 3a and b (Ti-Be sample) considering the deficiency method implemented with simulated nitrogen bubbles. (For interpretation of the references to colour in this figure legend, the reader is referred to the web version of this article.)

RBS spectrum considering the presence of nitrogen bubbles.

3.2.2. Zr-Be sample

Fig. 4 shows the results from the fit to the RBS spectrum measured for the Zr-Be sample after the nitrogen implantation. The elements

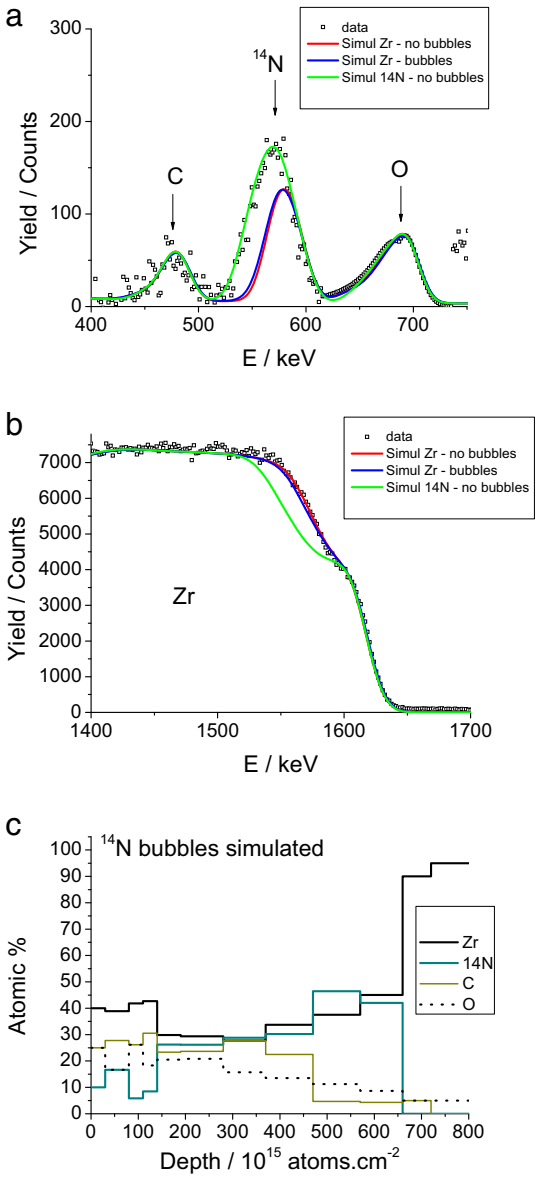

Fig. 4. a) – Partial RBS spectrum (C, ^{14}N, O region) taken for the Zr-Be sample after the ^{14}N implantation. The spectrum was fitted with DataFurnace code considering three situations. i) Green line (direct method): a good fit to the ^{14}N signal is obtained with a significant Zr yield reduction not described by experimental data, as shown in Fig. 4b. ii) Red line: deficiency method fit without considering the formation of nitrogen bubbles. The Zr signal is well-simulated (Fig. 4b), but the ^{14}N expected yield dropped by 45% as compared with the direct method fit (green line). iii) Blue line: deficiency method fit simulated with nitrogen bubbles. The Zr signal is well-simulated (Fig. 4b), but the ^{14}N expected yield dropped by 43% as compared with the direct method fit (green line).
b) – Partial RBS spectrum (Zr region) taken for the Zr-Be sample after the ^{14}N implantation. The spectrum was fitted with DataFurnace code considering three situations. i) Green line: direct method ^{14}N fit. ii) Red line: deficiency method fit without considering the formation of nitrogen bubbles. iii) Blue line: deficiency method fit simulated with nitrogen bubbles.
c) – Elemental depth profiles for Zr, ^{14}N, C and O obtained from the RBS spectrum fit of Fig. 4a and b (Zr-Be sample) considering the deficiency method implemented with simulated nitrogen bubbles. (For interpretation of the references to colour in this figure legend, the reader is referred to the web version of this article.)

considered in this fit are Zr, ^{14}N, C, O and Be comprised in 21 layers. The elemental depth profiles obtained from the fit to the RBS spectrum considering the presence of nitrogen bubbles is shown in Fig. 4c) for the first 11 layers. In this case, there is also no agreement between the direct and the deficiency method for ^{14}N quantification.

Considering a fit where no nitrogen bubbles are simulated, the ^{14}N

signal [green line in Fig. 4a) and b)] gives a retained fluence of [2.56 ± 0.03 (stat) ± 0.09 (syst)] × 10^{17} atoms·cm^{-2} (=26% of the nominal fluence) while the fit to the Zr signal [red line in Fig. 4a) and b)] gives a ^{14}N retained fluence of [1.42 ± 0.00 (stat) ± 0.06 (syst)] × 10^{17} atoms·cm^{-2} (=14% of the nominal fluence). The deficiency method thus gives a ^{14}N yield that is 45% lower when compared with the direct quantification of the ^{14}N signal. Including in the simulation bubbles of ^{14}N (10 nm radius, randomly distributed occupying a volume fraction that ranged from 0% to 55%), Fig. 4 (blue line) shows that there is almost no improvement: the ^{14}N retained fluence of [1.47 ± 0.00 (stat) ± 0.06 (syst)] × 10^{17} atoms·cm^{-2} (=15% of the nominal fluence), meaning that the discrepancy between deficiency method and the direct method decreased only by 2%, from 45% to 43%.

A possible explanation for this systematic inconsistency observed for the nitrogen yield in the implanted samples may be an oversimplified stopping power calculation. DataFurnace (and other similar codes) implement Bragg's rule for the stopping power cross sections calculations. This rule assumes that the stopping power of a compound is merely the summation of the stopping effects of each individual element, weighted by their abundance in the compound. The control samples TiN-Be and ZrN-Be have shown that this rule works well for TiN and ZrN, since good fits to the RBS spectra were obtained (see Fig. 2). For the implanted samples, the light gold colour presented after the ^{14}N implantations shows that a nitride compound was formed, so a good fit was also to be expected, especially after including the presence of nitrogen bubbles in the simulation, which are known to be formed in very high nitrogen fluence implantations. This failure in the expected values means that these nitrogen implantations induced a surface modification that is not well described by the actual stopping power models used in the simulation codes. This means that the deficiency method commonly used to determine nitrogen depth profiles and retained fluences gives wrong results. To better understand the discrepancies between the direct and the deficiency methods, it is planned to study these samples with SIMS + XPS (Secondary Ion Mass Spectrometry + X-ray Photoelectron Spectroscopy), which are independent of the stopping power. The Ti (or Zr) and N depth profiles obtained can be compared with RBS data and from here infer any corrections that may be applied in order to get a good agreement between the two methods.

4. Conclusions

The retained and depth distribution of ^{14}N resulting from very high fluence implantations in Ti and Zr was obtained by RBS analysis. Due to the use of thin Ti and Zr films, it was possible to determine the nitrogen depth distribution simultaneously and independently for each RBS spectrum from the direct nitrogen signal and from the reduction of the backscattered yield from Ti and Zr (deficiency method). Fitting the RBS spectra for both samples showed that there is no agreement between the two methods. Including in the fitting code (DataFurnace) the simulation of nitrogen bubbles reduced the discrepancy for the Ti-Be sample, but not for the Zr-Be sample. These discrepancies may be due to oversimplified calculations for stopping powers in compounds.

Acknowledgements

The authors gratefully acknowledge L. Rebouta from the Research Centre on Interfaces and Surface Performance (Guimarães, Portugal) for preparing the Ti, Zr, TiN and ZrN films. J. Cruz, H. Silva and A.P. Jesus acknowledge FCT-NOVA.

This research did not receive any specific grant from funding agencies in the public, commercial, or not-for-profit sectors.

References

[1] B. Schmidt, K. Wetzig, Ion Beams in Materials Processing and Analysis, Springer-Verlag, 2013.
[2] P. Budzyński, P. Tarkowski, E. Jartych, A.P. Kobzev, Evolution of mechanical properties in tool steel implanted with high energy nitrogen ions, Vacuum 63 (2001) 737–742.
[3] Y. Liu, X. Zu, S. Qiu, X. Huang, Improvement of tribological behavior of a Ti–Al–V alloy by nitrogen ion implantation, Rare Metals 25 (2006) 309–314.
[4] D. Shikha, U. Jha, S.K. Sinha, P.K. Barhai, K.G.M. Nair, S. Dash, A.K. Tyagi, S. Kalavathy, D.C. Kothari, Microstructure and biocompatibility investigation of biomaterial alumina after 30 keV and 60 keV nitrogen ion implantation, Surf. Coat. Technol. 203 (2009) 2541–2545.
[5] SRIM, web page www.srim.org , Accessed date: 10 January 2017.
[6] Y. Wang, M. Nastasi, Handbook of Modern Ion Beam Materials Analysis, MRS, 2010.
[7] T. Fujihana, Y. Okabe, K. Takahashi, M. Iwaki, RBS, AES and XRD investigations of high-dose nitrogen-implanted Ti, Cr, Fe, Zr and Nb sheets, Nucl. Instr. Meth. B (144) (1990) 669–672.
[8] K. Yabe, O. Nishimura, T. Fujihana, M. Iwaki, Characterization of the surface layer of various metals implanted with nitrogen, Surf. Coat. Technol. 66 (1994) 250–254.
[9] P. Budzynski, Long-range effect in nitrogen ion-implanted AISI 316L stainless steel, Nucl. Instr. Meth. B 342 (2015) 1–6.
[10] Goodfellow, web page www.goodfellow.com , Accessed date: 10 January 2017.
[11] J. Cruz, M. Fonseca, H. Luis, R. Mateus, H. Marques, A.P. Jesus, J.P. Ribeiro, O.M.N.D. Teodoro, C. Rolfs, Production and characterization of thin 7Li targets fabricated by ion implantation, Nucl. Instr. Meth. B 267 (2009) 478–481.
[12] N.P. Barradas, C. Jeynes, Advanced physics and algorithms in the IBA DataFurnace, Nucl. Instr. Meth. B 266 (2008) 1875–1879.
[13] S.L. Molodtsov, A.F. Gurbich, Simulation of the pulse pile-up effect on the pulse-height spectrum, Nucl. Instr. Meth. B 267 (2009) 3484–3487.